Vol. 33, No. 3 / March 2016 /© Journal of the Optical Society of America A A53

Dependence of chromatic responses in V1 on visual field eccentricity and spatial frequency: an fMRI study

DANY V. D'SOUZA,[1] TIBOR AUER,[1] JENS FRAHM,[1] HANS STRASBURGER,[2] BARRY B. LEE[1,3,*]

[1]*Max Planck Institute for Biophysical Chemistry, Göttingen, Germany*
[2]*University of Göttingen, Göttingen, Germany*
[3] *SUNY College of Optometry, Biological Sciences, New York, USA*
Corresponding author: Barry B. Lee, blee@sunyopt.edu

Psychophysical sensitivity to red-green chromatic modulation decreases with visual eccentricity, compared to sensitivity to luminance modulation, even after appropriate stimulus scaling. This is likely to occur at a central, rather than a retinal, site. Blood oxygenation level dependent (BOLD) functional MRI (fMRI) responses to stimuli designed to separately stimulate different afferent channels (red-green, luminance and short-wavelength [S] cone) circular gratings were recorded as a function of visual eccentricity (+/-10 deg) and spatial frequency in human primary visual cortex (V1) and further visual areas (V2v, VP). In V1, the spatial frequency tuning of BOLD fMRI responses became coarser with eccentricity. For red-green and luminance gratings similar spatial frequency tuning curves were found at all eccentricities. The pattern for short-wavelength cone modulation differed, with spatial frequency tuning changing more slowly with eccentricity than for the other two modalities. This may be due to the different retinal distribution with eccentricity of this receptor type. A similar pattern held in V2v and VP. This would suggest that transformation or spatial filtering of the chromatic (red-green) signal occurs beyond these areas.

OCIS codes: *(330.1720) Color vision; (330.4270) Visual system neurophysiology; (330.5510) Psychophysics.*

http://dx.doi.org/10.1364/JOSAA.33.000A53

1. INTRODUCTION

Visual abilities change over the visual field (see Strasburger et al. [1] for review). Most attention has been paid to achromatic (i.e. luminance modulated) stimuli; chromatic stimuli have been less well studied. Color perception in peripheral vision was classically considered to be poor, but with large enough stimuli, color naming in peripheral vision is as in the fovea [2-5]. However, chromatic discrimination is generally considered to be poorer in peripheral compared to central vision even after size scaling, especially for red-green sensitivity [6-11].

For achromatic gratings, foveal and peripheral visual performance can often be made similar if stimulus size is suitably increased and spatial frequency decreased for the peripheral stimuli [12-15]. Early work was concerned to relate such scaling to ganglion cell density and the area of V1 devoted to different eccentricities [15-17]. In reference to the cortical magnification factor M [18, 19] such stimulus scaling is usually referred to as M-scaling. The variation of the psychophysical scaling factor with visual-field eccentricity is typically described by a linear function that is characterized by its slope and x-axis intercept. The latter value has become to be known as that function's E2 value [20]. E2 values for many visual functions were summarized by Strasburger et al. [1]. For low-level function, most work has used achromatic (i.e. luminance modulated) stimuli, and M-scaling for chromatic stimuli may follow different rules.

Available evidence suggests Old-World primates performance is similar to humans on simple color vision and spatial tasks (e.g., [21, 22]). In primates, midget ganglion cells of the parvocellular (PC) pathway are thought to be the origin of the red-green channel for color vision, whereas small bistratified cells of the koniocellular (KC) pathway are one of the cell types which make up a substrate of the blue-yellow channel of color vision (see Lee [23] for review). For PC cells, red-green opponency results from antagonistic interaction of the middle- (M) and long-wavelength (L) cones, either +L-M or +M-L. In and near the fovea, a midget ganglion cell's center is driven by a single cone (e.g., an L-cone) via a midget bipolar cell, while the surround receives input either from a different cone type (e.g., M-cone; selective surround) or from mixed cone-types (mixed surrounds). Both schemes result in color opponency, although physiological evidence suggests at least some degree of cone selectivity in the surround near the fovea [24-30]. Beyond about 10 deg eccentricity, convergence of midget bipolar cells onto midget ganglion cells begins to occur so that, by 20 degree eccentricity, there is substantial convergence (10-20 bipolars per ganglion cell; [31, 32]. It was

proposed that the loss of red-green chromatic discrimination in peripheral vision is associated with random midget bipolar input to the midget ganglion cell center, which causes a loss of chromatic responsivity in midget ganglion cells [7, 9, 10, 33]. However, a substantial proportion of midget ganglion cells at eccentricities greater than 20 deg show |L-M| opponency that is just as pronounced as near the fovea [34, 35], although at higher eccentricity, physiological evidence does suggest loss of opponency [36, 37]. However, the psychophysical loss of red-green chromatic sensitivity is already pronounced at 10 deg eccentricity, where the one-to-one midget morphology is well maintained. This would suggest that the psychophysical sensitivity loss occurs beyond the retina. Although the relation of chromatic sensitivity with eccentricity has not been specifically studied in macaque lateral geniculate nucleus (LGN) many recordings at eccentricities greater than 10 deg (e.g., [38, 39]) have not noted any loss in chromatic responsivity in the parvocellular layers. Thus, it is difficult to avoid the conclusion that any loss in |M-L| psychophysical sensitivity in the periphery occurs at cortical sites.

Psychophysical sensitivity of M-scaled stimuli isolating the S-cone pathway also decreases with eccentricity more rapidly than sensitivity to achromatic stimuli, but not so much as with |M-L| stimuli [7, 40] The small-bistratified cells of the KC pathway receive excitatory input from the short-wavelength (S) cones opposed by some combination of the other two cone types (+S-(M+L)). However, one complicating factor is the difference between S-cone (and the associated ganglion cell) density and M- and L-cone densities as a function of eccentricity [41]. There are no S cones in a small patch of central fovea (10-20 arcmin); their proportion increases to around 7-9% at 5-7 deg eccentricity and thereafter remains stable. This would indicate that the usual magnification factor equation is not appropriate for S-cone mechanisms, and there is some psychophysical evidence for this [42, 43]. This factor has generally not been considered when designing M-scaled stimuli tapping the S-cone pathway.

There have been numerous reports on fMRI responses in V1 to chromatic modulation; both |L-M| and S-cone modulating stimuli yield vigorous responses [44-51]. There have also been studies of spatial frequency tuning of fMRI responses in V1, but mostly with respect to luminance responses [46, 52]. Two studies have been concerned with comparing luminance, |M-L| and S-cone responses in V1 and elsewhere [48, 53] at different eccentricities; we compare our results with these studies in the discussion.

We have previously reported on the temporal frequency tuning of V1 and further visual areas [51], in an attempt to locate a loss of high-temporal-frequency response to chromatic modulation by following chromatic fMRI signals through the visual pathways. PC and KC retinal ganglion cells respond to much higher temporal frequencies than can be detected psychophysically, so that a cortical loss of sensitivity is implicated. Here we attempt to specifically investigate a possible loss of peripheral chromatic sensitivity by measuring chromatic responses as a function of eccentricity. We expanded on previous studies in that we explored a broad range of spatial frequencies. This led us to consider possible differences in M-scaling of luminance, |M-L| and S-cone function with eccentricity.

Two features of the results are, firstly, that, compared to Lum responses, |L-M| responses are largely maintained at least up to 10 deg eccentricity in V1, and secondly, that the spatial frequency tunings of |L-M| and Lum responses are similar. Both these features appear to reflect properties of the retinal input rather than psychophysical performance. Spatial frequency tuning of S-cone responses follows a different pattern. It was more difficult to draw conclusions for visual areas beyond V1, but at least in V2v and V3v a similar pattern of results is likely to hold.

2. METHODS

A. Subjects

Three healthy volunteers (1 female and 2 male; mean age 26 years) participated in the study. All subjects had normal visual acuity and were color-normal; normalcy for color vision was confirmed by the Farnsworth Munsell 100-Hue Test. Informed written consent was obtained from subjects prior to participation in each experimental session. All experimental procedures strictly conformed to the institutional guidelines. Each subject participated in two experimental sessions. In the first, we used standard retinotopic mapping procedures to identify boundaries of the primary visual cortex (V1) and further areas. In the second, we measured fMRI responses to selective stimulation of the chromatic (|L-M| cone-opponent and S-cone) and luminance pathways using circular grating stimuli of various spatial frequencies.

B. Visual display system

Visual stimuli were generated using a VSG ViSaGe system (Cambridge Research Systems Ltd., Rochester, UK) and were presented by a SANYO, PLC-XT 11 LCD projector (pixel resolution 1024 × 768, frame rate 80 Hz, mean luminance 126 cd/m2) on a translucent screen mounted on the top of the MRI headcoil in front of a 45° tilted mirror (Schäfter & Kirchhoff, Hamburg, Germany). The visual display subtended a visual angle of approximately 28° horizontally and 21° vertically. For retinotopic mapping experiments, the visual stimuli were generated using a stand-alone software tool (StimulDX, Brain Innovation, Maastricht, The Netherlands) based on the Microsoft DirectX library. The VISaGe system has 14 bit resolution and after gamma correction ca. 8 bit, i.e., 0.5%.

C. Calibration

The LCD projector system was calibrated for luminance and chromaticity by defining gamma curves and spectral properties separately for each of the three RGB color channels. For gamma correction within the scanner, we transmitted local luminance values by a fiber optic cable to a digital luminance meter (Mavo-Monitor USB, GOSSEN Foto- und Lichtmesstechnik GmbH, Nürnberg, Germany) located outside the scanner, following the procedures described by Strasburger, Wüstenberg and Jäncke [54] to determine the relationship between the digital input and resulting luminance. Attenuation of each primary by the fiber optic cable was separately checked and corrected. The luminance values were entered manually into the VSG gamma calibration software. The chromaticity of the projector output was calibrated with a PR-650 Spectra Colorimeter (PhotoResearch Inc., Chatsworth, MA) using a mirror arrangement. The CIE chromaticity coordinates for the R, G, and B primaries were then entered into the VSG software before the gamma-corrected look-up-tables (LUTs) were

generated. To check the temporal characteristics of the LCD projector we used a photodiode in combination with an operational amplifier, and a digital oscilloscope (TDS 2024B, Tektronix, Beaverton, OR).

D. Visual Stimuli

The stimuli were contrast-reversing (2 Hz sinusoidal modulation) circular sine-wave gratings, spanning a diameter of 21° visual angle, with a central cross (1° in diameter) that was used for the fixation task. Stimuli of various spatial frequencies (SFs of 0.27, 0.55, 1.09, 2.2, and 4.4 cpd) were used. In addition to grating stimuli with a fixed SF within the pattern, we also tested an approximately M-scaled circular grating where the central SF (4.4 cpd) was scaled across the radius, resulting in 0.16 cpd at the stimulus perimeter. Fig, 1A illustrates the spatial layout of stimuli; for simplicity only two spatial frequency examples are shown. Three types of stimuli, '|L-M|', 'Lum', and 'S', were designed to individually activate |M-L| cone-opponent, luminance, and S-cone postreceptoral pathways, respectively. The |L-M| and S stimuli were isoluminant. We constructed stimuli using the Smith and Pokorny 10° cone fundamentals [55]. Cone fundamentals were multiplied with the emission spectra of the red, green, and blue spectral outputs of our LCD projector, resulting in a calibration matrix. The matrix values represent the spectral absorptions of the S-, M-, and L-cones to red, green, and blue lights, respectively. Using these cone-excitation values, we computed the chromaticity values for pathway-selective stimuli. In the results described, the mean CIE (x,y) chromaticity coordinates for the |L-M|, Lum, and S-cone conditions were (0.51, 0.47), (0.51, 0.47), and (0.26, 0.22), respectively. We also carried out extensive preliminary experiments in which stimuli for all conditions were modulated around equal-energy white. This resulted in lower cone contrasts, and fMRI signals were weaker and less reliable, especially in extra-striate visual areas. However, the pattern of results was similar to those presented here. The stimuli had a mean luminance of 127 cd/m2, and modulation of the LCD primaries was modified to give a mean cone contrast of 29%, calculated as the vector length (square root of the sum of squares) of individual cone-contrasts [45]. Isoluminance points for the chromatic stimuli were obtained for each observer using the minimum-motion technique inside the MR scanner in the same experimental setup. In practice, for all subjects tested, isoluminance values were close to those of the standard CIE observer.

E. Experimental design

Each subject participated in three experimental runs; each run lasted 10 minutes. In a typical run one of the three stimulus gratings (|L-M|, Lum, or S) was shown at six different spatial frequencies (0.27, 0.55, 1.09, 2.2, 4.4, as well as 4.4-cpd scaled), using a block-design paradigm (Fig. 1B) similar to that used by Henriksson, Nurminen, Hyvärinen & Vanni [52]. Each experimental run (|L-M|, Lum, or S) commenced with a 24 s control period (data from the first 12 s were discarded in the analysis), followed by 6 stimulus cycles. Each cycle (96 s) in turn consisted of 6 stimulus blocks (12 s each) and a control block (24 s). In each stimulus block we presented contrast reversing gratings at one of the given spatial frequencies. The order in which these were presented was pseudo - randomized within each cycle and balanced

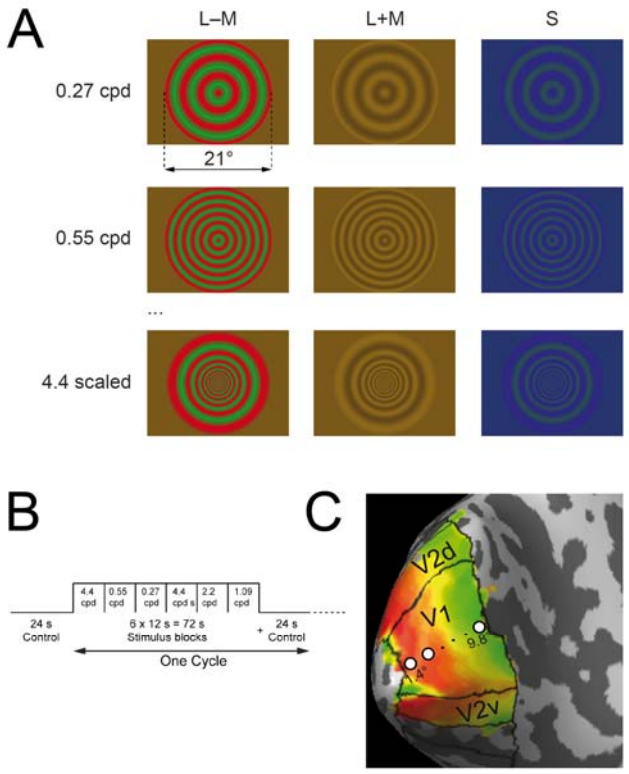

Fig. 1. A, Pathway-selective stimuli at various spatial frequencies (SFs). Circular sine-wave gratings subtending a visual angle of 21 deg were used. The pathway-selective stimuli are shown in three columns. Upper two rows show example spatial frequencies. Row three shows scaled stimuli with a central SF of 4.4 cpd decreasing to 0.16 cpd at the stimulus perimeter. B. An experimental run, commenced with a control period (mean-chromaticity screen) followed by 6 cycles. Each cycle consisted of 6 stimulus blocks and a control block. In each stimulus block the contrast of the grating was modulated at one of the six different SFs. The order in which the SFs were presented was pseudo-randomized within each cycle. C. Identification of the visual cortices (V1) and eccentricity maps. Boundaries separating V1 from the dorsal and ventral parts of area V2 are shown on a reconstructed cortical surface (left hemisphere) of a single subject. Eccentricities are color coded, with near-foveal regions represented in reddish-orange and higher eccentricities having yellowish-green representation. White circles correspond to regions of interest (ROIs) at the following eccentricities: 1.4, 2.2, 3.0, 3.8, 4.6, 6.3, 8.1, and 9.8 deg.

across the experimental run. During the control blocks, no stimulus appeared and a blank screen was shown with the same mean chromaticity and luminance as the grating stimulus. Each run lasted 600 s (300 functional volumes, TR = 2 s). Since each run was limited to one condition (|L-M|, Lum, or S), mean chromaticity and luminance was the same throughout the run.

To maintain attention and fixation during the stimulus and control blocks, a small fixation cross was luminance-modulated (2 Hz sinusoidal) with 50 % Michelson contrast, and at random intervals was replaced by a black cross.

Subjects were asked to detect the occurrences of the black fixation cross during the experimental run. All subjects detected above 95% of the dimming events.

F. Magnetic resonance imaging (MRI)

All imaging studies were performed on a 3 T scanner (Magnetom Tim Trio, Siemens, Erlangen, Germany) using a 12-channel receive-only phased-array head coil. For anatomical data, a high-resolution T1-weighted 3D data set (MPRAGE, 1×1×1.1 mm3) was acquired in each retinotopy session. These images were used to reconstruct the cortical surfaces for mapping and visualization purposes. At the beginning of each main experimental session, T1-weighted 3D FLASH images (1×1×1 mm3) were acquired. These anatomical images served to coregister the functional data with the MPRAGE data acquired in the retinotopy session. For functional data, blood oxygenation level dependent (BOLD) fMRI responses were measured with use of a T2*-sensitive gradient-echo echo-planar imaging (GE-EPI) technique with an in-plane resolution of 2×2 mm2 (repetition time (TR): 2000 ms, echo time (TE): 36 ms, flip angle: 70°, acquisition matrix: 96×96). Functional volumes comprised 22 consecutive sections of 4 mm thickness, oriented approximately perpendicular to the calcarine fissure and covering early as well as higher visual areas in the occipital lobe.

G. MRI data processing and analysis

Data analysis was performed using BrainVoyager QX 1.10 (Brain Innovation, Maastricht, The Netherlands). The anatomical volumes (MPRAGE) acquired during the retinotopy sessions were first interpolated to a 1×1×1 mm3 isotropic resolution. Subsequent processing steps included correction for intensity non-uniformity, AC-PC transformation, and finally transformation of the data to a standard stereotaxic space (Talairach transformation). We used the Talairach transformed data to reconstruct cortical surfaces at the white-gray matter boundary. These surface reconstructions for each hemisphere were then inflated. Anatomical volumes acquired during the second sessions were automatically aligned to MPRAGE data from the first sessions. Preprocessing of the functional data included deletion of the initial 6 volumes (that were prepended to allow longitudinal magnetization to reach a steady state), 3D-motion correction (also including intra-session alignment), slice-time correction, temporal high-pass filtering (3 cycles/run), linear-trend removal, spatial smoothing with a Gaussian kernel (full width at half maximum 4×4×4 mm3). After preprocessing, functional data were co-registered to the anatomical volume (FLASH) acquired at the beginning of the same session, and subsequently transformed into Talairach space.

H. Identification of visual areas

Retinotopic mapping was performed for each of the three subjects in separate scanning sessions. Standard phase-encoded retinotopic mapping procedures were employed to map the visual field eccentricities (expanding rings) and to distinguish boundaries separating the visual areas V1 and V2 (polar angle mapping) [56, 57]. In brief, for eccentricity mapping, six ring stimuli (checkerboards, scaled for eccentricity, high contrast, 8.33 Hz reversal) were presented sequentially in 10 s duration blocks. A cross-correlation analysis was performed [58, 59]. Eccentricity maps were also confirmed with traveling wave stimuli [56, 57]. In addition, we also obtained maps of the horizontal and vertical meridian by using meridian-specific stimuli. Briefly, high contrast reversing (8.3 Hz) wedge (30 deg) checkerboards were used. Horizontal and vertical meridian stimuli were alternated in blocks of 12 s duration, over 12 cycles. Again, a correlation method was used to delineate area boundaries. These confirmed boundaries obtained using the standard rotating wedge stimuli for polar angle measurements [57, 60, 61].

I. Region of interest (ROI) analysis

ROIs with a mean size of 25 voxels were defined corresponding to a location near the fovea (1.4° eccentricity) and at increasing visual field eccentricities in primary visual cortex (V1). Each ROI had dimensions of 2×2×2 mm3, ca 25 voxels. The spatial profile of the stimulus corresponds to 40-45 mm of cortical distance in V1, and the ROIs were located almost abutting along this axis as illustrated in Fig. 1C. We note that it is unlikely that the hemodynamic response derives solely from cortex within each ROI, and some blurring is inevitable. We thus considered using an arc of cortex as a ROI, but this would have led to a further potential lack of resolution. To estimate the strength of the fMRI response within each of these ROIs, we performed a General Linear Model (GLM) analysis separately for each hemisphere. To do so, we first extracted the mean fMRI time course of a given ROI for a given experimental run, corresponding to each of the three stimulus conditions (|L-M|, Lum, or S), by averaging over all voxels. In the subsequent step, the time course was normalized using the z-value-transformation. Next, the GLM with 6 predictors (corresponding to the 6 SF conditions; see below) and a baseline (control block) was fit to the normalized time course. The time course of the predictors was computed from the stimulation protocol and was convolved with the two-gamma hemodynamic-response function [62]. In the GLM equation, each predictor time course is associated with a coefficient or beta weight β, quantifying its contribution in explaining the ROI time course. The six beta weights in this context reflect the strength of the fMRI response at 5 SFs (0.27, 0.55, 1.09, 2.2, 4.4 cpd), and a spatial-frequency scaled stimulus (4.4 cpd scaled). A similar procedure was adopted with further visual areas.

J. Spatial frequency tuning curves

For the tested eccentricities the fMRI response, averaged across subjects, was plotted as a function of SF of the circular gratings for three stimulus conditions: |L-M|, Lum, and S, respectively. To characterize the SF tuning properties at these eccentricities, we fitted Gaussian functions to the data with a procedure similar to that described by Henriksson et al. [52]. The four-parameter Gaussian function used in the analysis is given by

$$R = R_0 + R_1 \exp\left(-\frac{(f-\mu)^2}{2\sigma^2}\right)$$

where R is the fMRI response (beta-weight) at a particular spatial frequency f, and R0, R1, and μ, are parameters that were estimated using the Marquardt-Levenberg minimization algorithm provided in Sigmaplot®. For each data set with band-pass tuning characteristics, the fitted parameter μ indicated the optimal SF; for the tuning data with low-pass or

high-pass tuning characteristics, the lowest or the highest SF, respectively, was considered as the optimum SF.

3. RESULTS

A. Responsivity as a function of eccentricity in V1

The fMRI response to selective stimulation of the chromatic (|L-M| and S-cone) and luminance pathways were measured in ROIs corresponding to the near-fovea (1.4 deg) through higher eccentricities up to approximately 10 deg, in retinotopically-mapped primary visual cortex (V1). We measured responses to circular sine-wave gratings at a range of spatial frequencies and also to M-scaled circular gratings, where the spatial frequency increases across the radius in an attempt to match the cortical magnification factor.

In Fig. 2, fMRI BOLD responses in V1, averaged across six hemispheres, are plotted for a set of spatial frequencies as a function of visual field eccentricity. The data show that V1 responds robustly to all stimuli, with the strongest responses to |L-M| cone-opponent, compared to luminance (Lum) and S-cone stimulus conditions across all spatial frequencies. This result is in line with previous fMRI reports on cortical processing of chromatic modulation [44-46, 49]. There are interactions between spatial frequency and eccentricity for all conditions. Thus, for a spatial frequency of 0.27 cpd (Fig. 2A), both |L-M| and luminance responses are largest at higher eccentricities whereas at the highest spatial frequency measured (4.4 cpd), the maximum response is at the lowest eccentricity. Eccentricity-dependent changes are also seen with S-cone stimulation. These shifts in maximum response are consistent with a coarser representation of visual space with increasing eccentricity.

We tested an M-scaled grating stimulus to try and equalize response amplitude across eccentricity (Fig. 2, lower right). The scaled stimulus (4.4 cpd at the center and 0.16 cpd at the perimeter) was used for the three stimulus types. For |L-M| and Lum, the scaling was only partially effective; although the data show consistently strong responses with a flatter characteristic, although there is a slight inverse-U shape; curves for both these conditions were very similar in shape. For the S-cone stimulus, the shape of the curve deviates from the other two condition, a result we return to below.

To compare these changes more directly between channels, the data were replotted, normalized in each case to the peak response for that condition at that eccentricity (Fig. 3A). The |L-M| and Lum curves generally show a similar pattern as a function of eccentricity for all spatial frequencies. There are some deviations from this finding. The 0.27 cpd curve shows a larger response for |L-M| and S cone stimuli close to the fovea compared to the respective Lum stimulus. This is consistent with a low-pass spatial frequency response of chromatic pathways compared to luminance responses, as seen both physiologically at precortical levels [63, 64] and psychophysically. For the scaled stimulus (lower right), the responses are not entirely independent of eccentricity. However, the shapes of the curves for |L-M| and Lum are similar. Both differ at higher eccentricities compared with the S-cone stimulus. This issue is taken up below.

To quantify this further, we plotted the ratio between Lum and |L-M| responses for each spatial frequency in Fig. 3B. Apart from the different shape for 0.27 cpd noted above (due to a relatively weak Lum response at low eccentricities), and

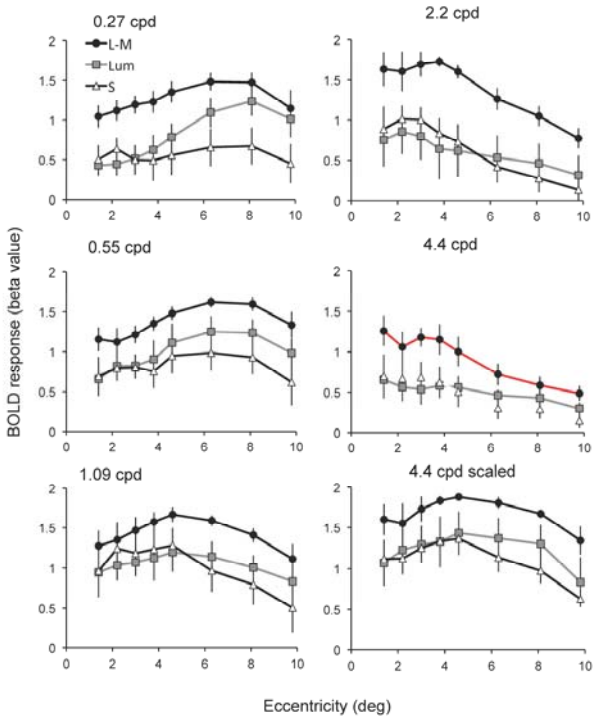

Fig. 2. BOLD fMRI response as a function of visual field eccentricity in V1, averaged over six hemispheres, are plotted as a function of visual field eccentricity for stimulation of the three post-receptoral pathways:. Each plot shows eccentricity-dependent responses at a different spatial frequency, and to the scaled stimulus. The data show that responses depend on condition and vary with stimulus spatial frequency and eccentricity.

for 4.4 cpd at high eccentricities (where S-cone responses were weak), ratios do not change systematically with eccentricity. Taking all data together, there was no significant effect of eccentricity on the Lum/|L-M| ratio (ANOVA test using GLM: $P = 0.068$).

For the S-cone stimuli, however, the results differed from the other two conditions. Responses fall off more rapidly at higher spatial frequencies as a function of eccentricity. This is seen in Fig. 3C, which shows the ratio of (Lum)/S-cone responses; there is a consistent and pronounced increase in ratio with eccentricity, especially for spatial frequencies above 1.09 cpd (at 2.2 and 4.4 cpd). This difference was statistically significant (ANOVA test using GLM: $P < 0.001$). A similar result was found when S-cone responses were compared to the |L-M| responses (not shown). We also performed an extensive series of preliminary observations with stimuli modulated around the white point, with similar results. However, we focus here on the data from the concatenated block design, which yielded more reliable results.

These data suggest that, especially for |L-M| and luminance stimuli, a similar spatial-frequency tuning pattern is found across eccentricities, and implies that for |L-M| opponent stimuli, responsivity is well maintained in the peripheral representation of V1. The S-cone responses show a different pattern to the other conditions and we now show

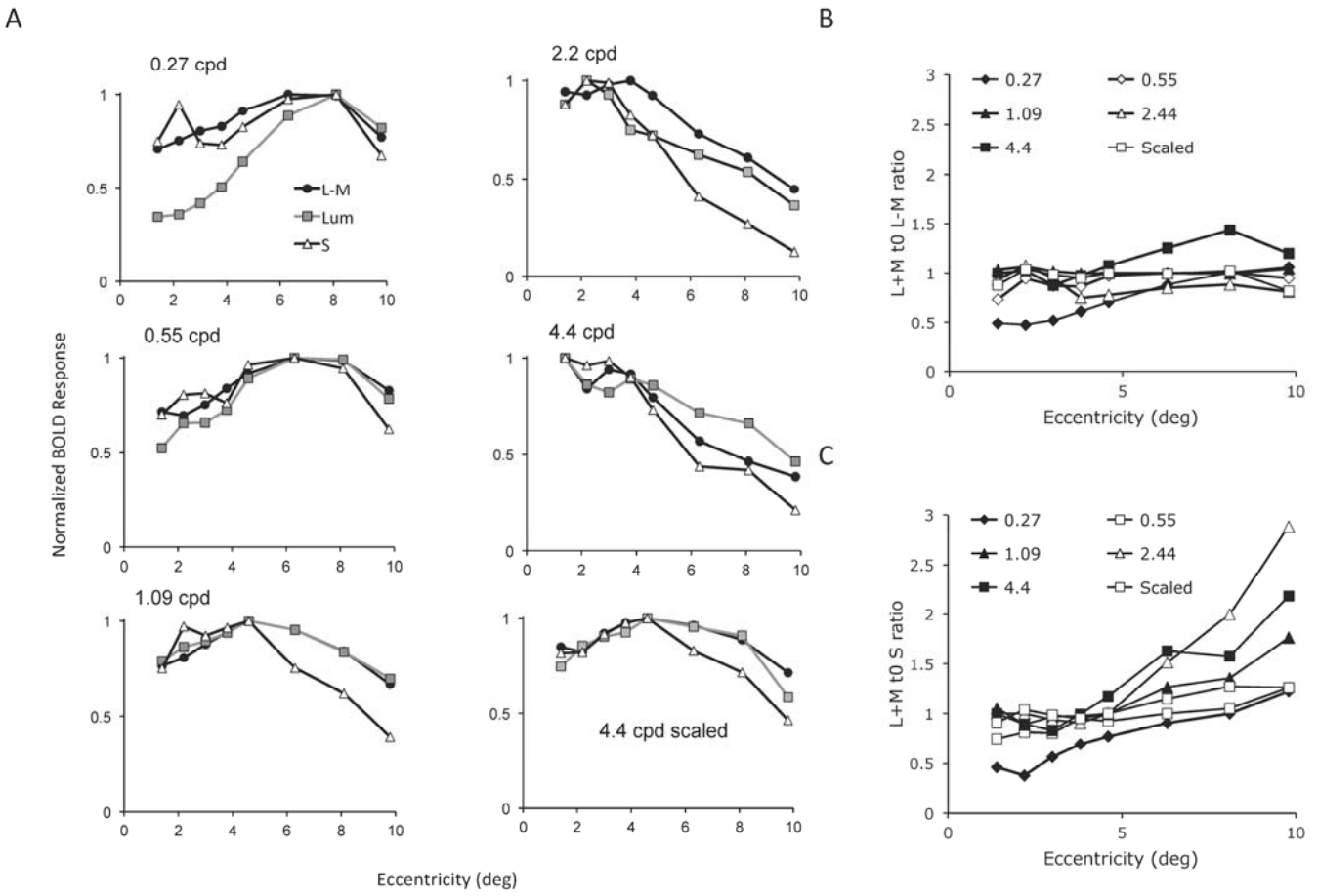

Fig. 3. A. BOLD fMRI responses normalized to the peak value for each condition is plotted against eccentricity for the different spatial frequencies. This facilitates comparison between different conditions. B. To further pursue this comparison, ratios of normalized responses between Lum and |L-M| are plotted and between Lum and S cone are plotted.

that this may be associated with spatial frequency tuning at different eccentricities.

B. Spatial frequency tuning curves in V1: estimation of E_2 values

To characterize the spatial-frequency tuning properties we estimated the optimum spatial frequency at each eccentricity. Three examples are shown in Fig. 4 (left column; circles: 1.4 deg; squares: 4.6 deg; triangles: 9.8 deg), for the three pathways (|L-M| cone-opponent, luminance (Lum), and S-cone. We fitted Gaussian functions to the data (on a linear spatial-frequency axis), following the fitting procedure explained in Henriksson et al. [52]. For |L-M| (Fig. 4A) and luminance (Lum) stimulus conditions (Fig. 4B), the tuning curves were band-pass to a greater or lesser extent for all eccentricities, with the peak spatial frequency declining with increasing visual field eccentricity. Similar findings were reported in Henriksson et al.'s study [52], which just employed achromatic stimuli. For the S-cone stimulus (Fig. 4C), the tuning curves were also band-pass; their peak spatial frequencies lay closer to each other, however. We note that, in the periphery (e.g. at 9.8 deg), low spatial frequency stimuli are required to obtain responses equivalent to those obtained centrally at higher spatial frequencies (e.g. at 1.4 deg). This was reflected in the sequential leftward shift of the tuning functions as eccentricity increased.

Because these tuning functions look similar, their eccentricity dependence can be investigated by scaling [16, 42, 65]. The SF scaling factors are shown in Fig. 4, right column, for the three stimulus conditions. We then fitted linear regression lines to these values. The resulting linear relationships between eccentricity and spatial-frequency normalization factor can be summarized by their respective horizontal intercept, E2, and slope of the fitted straight line [1, 20, 66, 67]. These values are displayed on each plot, together with r^2. Note the negative abscissa intercept and linear behavior, which is consistent with the cortical magnification hypothesis [1, 15–20]. The scaling functions for the |L-M| and Lum mechanisms were steeper than those for the S-cone mechanism. The |L-M| slope is slightly steeper than the Lum slope (4D vs. 4E), but the difference falls just short of significance (p=0.0528, t test). However, the slope for the S cone stimulus is much shallower than for the other two

conditions at high significance level ($p<0.001$, t test). This finding is effectively a reformulation of the data in Fig. 4C.

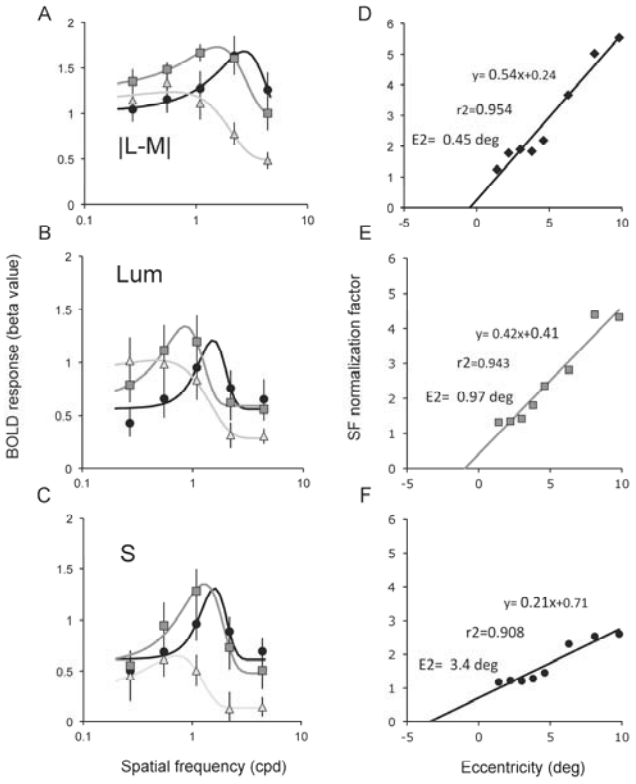

Fig. 4. Spatial frequency tuning functions in V1 at different eccentricities. A-C. BOLD fMRI responses as a function of spatial frequency at different eccentricities (o: 1.4 deg; □: 4.6 deg; Δ: 9.8 deg) for stimulation of the three pathways: (A) |L-M|, (B) Lum, and (C) S, respectively. For quantification of the optimum spatial frequencies, Gaussian functions (solid line: 1.4 deg; dotted line: 4.6 deg; short dashed line: 9.8 deg) are fitted to the data. Right column: Spatial frequency scaling factors required for normalizing the three scaling functions at eccentricities 1.4, 4.6, and 9.8 deg to that at 1.4 deg by matching their optimum spatial frequency values: |L-M|, Lum, and S, respectively. Straight lines are fitted to the data. E2 value is the eccentricity axis intercept.

The difference between S-cone, and Lum and |L-M| data, may be related to the different receptor densities across eccentricity in these pathways, a topic taken up in the discussion. Taken together, the data in Figs. 3–5 suggest that |L-M| responses in V1 remain robust up to 10 degrees eccentricity. We now briefly consider responses in other visual areas.

C. Responses as a function of eccentricity in areas beyond V1

We restricted analysis of eccentricity-related responsivity to ventral areas (V2v, V3v and V4), since the phase-related eccentricity mapping was better defined for these areas. There are indications that there may be some enlargement of the foveal representation in these areas [68-71]. However, we used the eccentricity maps generated with annuli to give an indication of eccentricity and we did not attempt to take such considerations into account.

Fig. 5A shows the amplitude of the BOLD fMRI signal as a function of eccentricity at different spatial frequencies in V2v. As in V1 (Fig. 2), robust responses are present to |L-M| (and S-cone) as well as to achromatic (Lum) stimulation. However, the markedly larger responses to |L-M| stimulation (closed circles) as compared to the other modalities (Lum and S cone) are less apparent and are confined to frequencies of 2.2 cpd and above (and relative to S-cone responses at 2.7 cpd). This was also the case in further ventral areas and is taken up at the end of this section.

The changes in spatial-frequency tuning with eccentricity observed in V1 are also present. For example, the responses to 0.27 cpd are largest at higher eccentricities but at 4.4 cpd the largest responses are closer to the fovea. That change appears common to |L-M| and achromatic (Lum) stimulation, whereas the pattern for the S cone is again different. This was made clearer when data were plotted as a function of spatial frequency to obtain tuning curves (not shown). We attempted to analyze the data by fitting tuning curves as for V1 (i.e. as in Fig. 4). However, this proved unsatisfactory since, with an optimum response typically occurring around 1 cpd or lower, the peaks were not always well defined; fitted curves were poorly constrained because the lowest spatial frequency tested (0.27 cpd) did not capture the curve's low spatial frequency roll-off of the curve. This is probably due to the larger receptive field sizes observed in V2 and further ventral visual areas [72, 73].

To further analyze these changes, we performed the same ratio calculation of BOLD fMRI responses as in Fig. 3B,C. This analysis is shown in Fig. 5B where these ratios are, as before, plotted as a function of eccentricity. As in V1, there is little systematic trend in the relative strengths of |L-M| and Lum signals with eccentricity over the different conditions (ANOVA test using GLM: $P = 0.435$). On the other hand, the ratios for Lum-cone relative to S-cone stimulation increase significantly with eccentricity at the higher spatial frequencies, i.e., S-cone responses become relatively weaker (ANOVA test using GLM: $P < 0.001$). This is consistent with different eccentricity scaling for S-cone mechanisms than those depending on the L and M cones, as was shown in Fig. 4 for V1. We did not pursue this further, since there may be some uncertainty as to eccentricity scaling in V2 as compared to V1, as noted above.

Fig. 6 shows the corresponding analyses for area V3v. Eccentricity functions for all spatial frequencies are shown in Fig. 6A. A similar pattern is seen as for V2v. There is the same interaction between spatial frequency and eccentricity as in the earlier areas. A ratio analysis is shown in Fig. 6B. For the comparison of achromatic Lum to |L-M|, the data just reached significance (ANOVA test using GLM: $P = 0.049$) However for the comparison of Lum to S, the data were highly significant (ANOVA test using GLM: $P = 0.002$). The data shown in Figs. 5 and 6 suggest that no substantial difference in the dependence of |L-M| and achromatic (Lum) signals with eccentricity develops from V1 to V3v. Also, the difference in S-cone signal-scaling with eccentricity is maintained.

We also attempted a similar analysis for V4 (not shown). It should be noted that the representation of the visual field in V4 in human is a matter of dispute (e.g. [69, 74-76]; reviewed

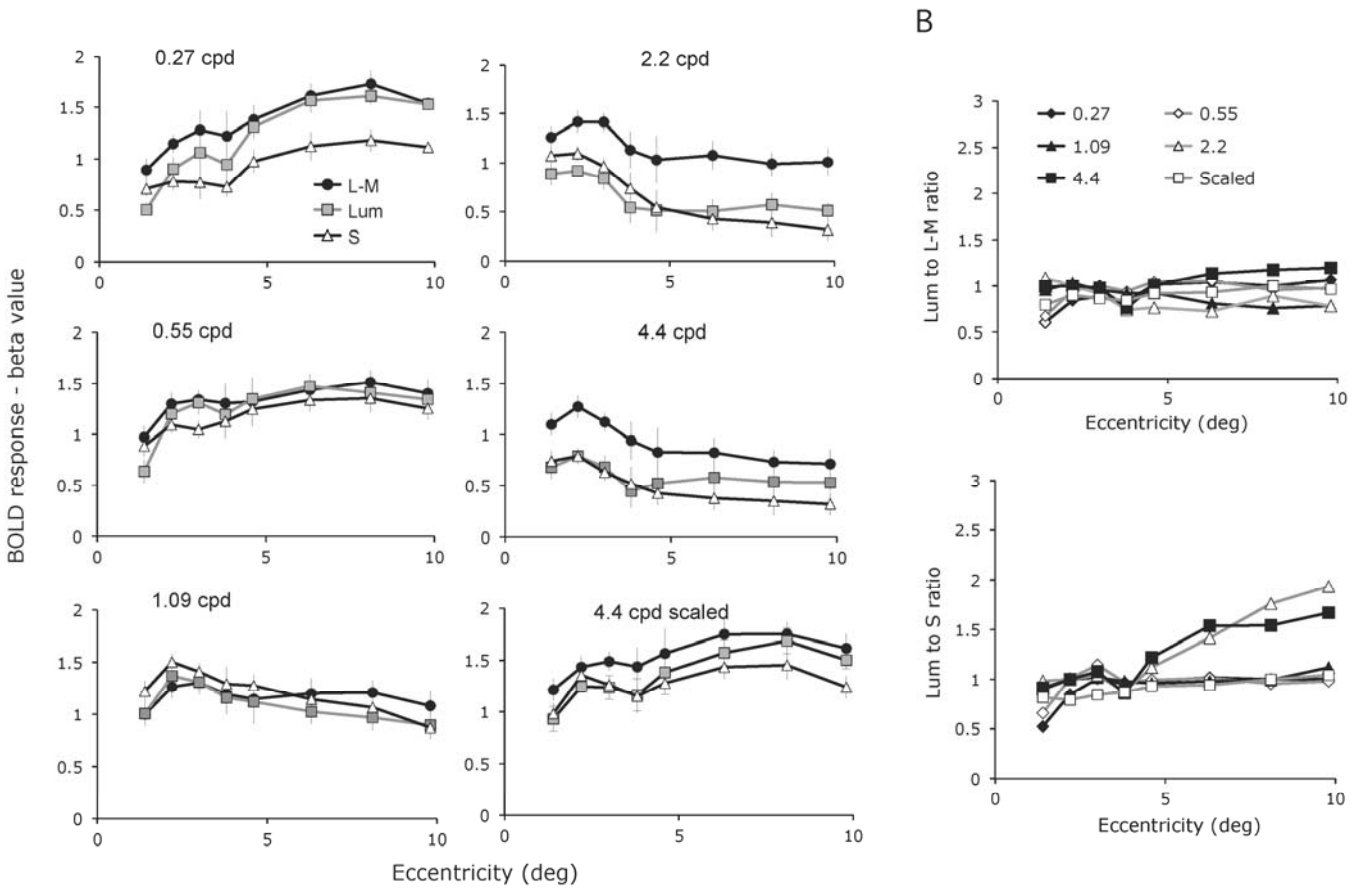

Fig. 5. Responsivity in V2v as a function of visual field eccentricity. A. BOLD fMRI responses are plotted against eccentricity for the different spatial frequencies. Similarities to the response pattern in V1 are apparent. B. Ratios of BOLD fMRI responses to Lum over |L-M| and S-cone responses, respectively.

in [77]. We obtained robust responses for all conditions. A different pattern appeared to be present in these results compared to V1, V2V and V3v. It should be noted that the representation of the visual field in V4 in human is a matter of dispute (e.g. [69, 74-76]; reviewed in [77]. So, due to the uncertainty of retinotopic organization in V4, we are cautious in interpreting these data, but it appears that the consistent pattern observed in V1, V2 and V3v is changed, with more similar responses between color channels.

4. DISCUSSION

A. The BOLD fMRI signal in relation to eccentricity

We measured BOLD fMRI responses to stimuli designed to selectively stimulate the different afferent retino-geniculo-cortical pathways, a neurophysiological 'bottom up' rather than a 'top-down' approach, in which fMRI responses depend on behavioral or cognitive contexts. Psychophysical sensitivity to red-green chromatic modulation is commonly held to decline more steeply toward the peripheral visual field than does luminance sensitivity or sensitivity to S-cone stimuli; it was proposed this might have a retinal basis in the changes of midget morphology with eccentricity [6-9]. However, electrophysiological measurements have shown that red-green responsitivity of PC cells is well maintained up to quite high eccentricities (>20 degrees) [34, 35]. From anatomical studies it is further evident that the one-to-one connectivity of the midget pathway is maintained up to ca. 10 deg and thereafter declines only gradually [78]. Psychophysical loss of sensitivity is already marked at 10 deg eccentricity. There has been no direct study of eccentricity-dependence and chromatic properties at the LGN level, but LGN studies (e.g., Derrington et al. [38]) have recorded extensively from 0-15 deg and have not noted any change in |L-M| opponency. This would implicate a cortical site in the sensitivity loss.

The eccentricity-dependent chromatic (|L-M| cone-opponent and S-cone pathways) and luminance responses are compared in Figs. 2–4 for V1. In our data, there was little or no difference in |L-M| relative to the achromatic (Lum) response as a function of eccentricity, as evident in Fig. 3. This would suggest that any loss of |M-L| psychophysical sensitivity in the periphery does not occur in V1, and data in Figs. 5 and 6 suggest a similar conclusion for V2v and V3v. There are, however, spatial frequency-dependent differences

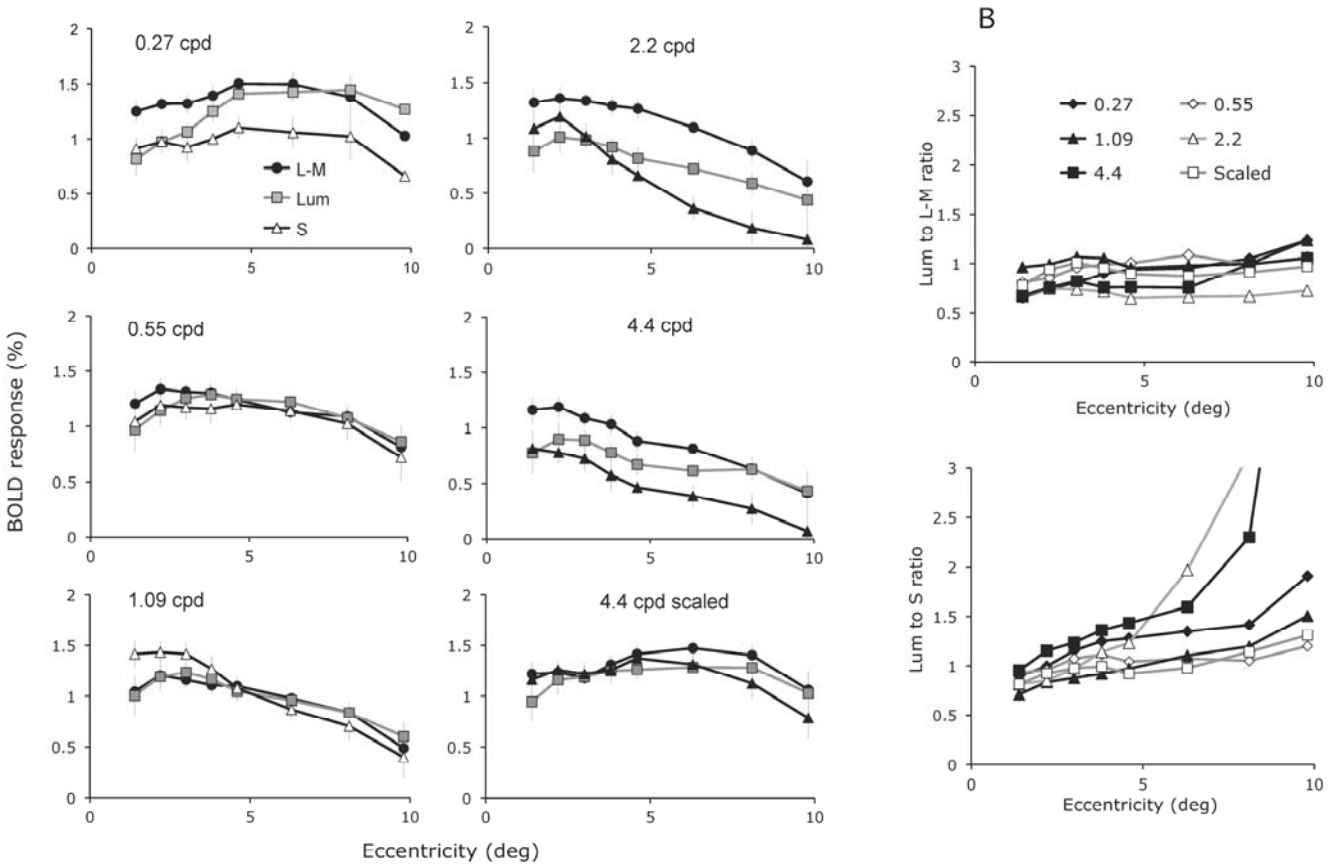

Fig. 6. Responsivity in V3v as a function of visual field eccentricity. A. BOLD fMRI responses are plotted against eccentricity for the different spatial frequencies. Similarities to the response pattern in V1 are apparent. B. Ratios of BOLD fMRI responses to Lum over |L-M| and S-cone responses.

between S-cone responsivity and responsivity to the other two conditions.

Two previous fMRI studies [48, 53] found some decline in |M-L| responses with eccentricity in V1, relative to the other two modalities. In the former ([48]; their Fig. 9), two of their eight subjects showed no decrease in |L-M| response with eccentricity, and another two showed only a minimal decrease. Also, in that study a fixed, low spatial frequency (0.5 cpd) was used. Our data (Fig. 3) show some spatial frequency-dependent effects that could lead to such a result. In the latter study [53], checkerboards were used, for which the spatial frequency spectrum is complex. In one case (their Fig. 5), S cone responses are compared to |L-M|. In view of the different spatial tuning of the S-cone signal compared to the other two conditions, this comparison may be misleading. Although our data cannot rule out some loss of |M-L| responsivity with eccentricity, responsivity seems well maintained. In any event, we have indications of spatial frequency-dependent effects when comparing the different conditions, and this indicates a more nuanced approach is required compared to these earlier studies. Mullen et al. [79] suggested that fMRI responses to S-cone stimulation, relative to L- and M-cone responses, are amplified in V1 as compared to LGN. Since our data suggest a complex relation between spatial frequency, S-cone signal, and eccentricity, this makes the hypothesis of an amplification of the S-cone signal more difficult to evaluate.

One difficulty in this analysis is that the relation of BOLD responses to psychophysical threshold is uncertain. Mullen et al. [48] found a better correlation of the BOLD signal with a cone-contrast metric than with a threshold-based metric. This indicates a relation of the BOLD response to activity in the afferent pathways (rather than to perceptual content). A second issue is the magnitude of any decrease of |M-L| psychophysical sensitivity with eccentricity, compared to the other two channels. We return to this issue below.

Stimuli were modulated around different mean chromaticities depending on the pathway to be isolated. This permits using relatively high cone-contrasts. Other investigators have modulated about the white point [48, 53], which lessens the cone contrasts available. In terms of pathway isolation, the mean chromaticity used is not thought to affect low-level psychophysical results. In a series of preliminary experiments, some measurements were made with stimuli modulated about equal-energy white. The general pattern of results obtained was similar to those described here. However, use of high cone-contrast stimuli and a pseudo-randomized stimulus block design yielded the

most reliable results with the least inter-individual variability, and these experiments form the basis of the results section. The spatial frequency tuning of |L-M| and Lum responses, and its relation to eccentricity, appeared to be similar (Fig. 4) and similar to the tuning curves for luminance gratings in Henriksson et al. [52] for different eccentricities. For luminance, spatial-frequency tuning curves near the fovea had a band-pass character as these authors describe. The tuning curves for the chromatic gratings were less band-pass in shape (Fig. 4).

Based on the present results, the response properties of V2v and V3v qualitatively resemble the V1 data. As in V1, there was a foveal preference for higher spatial frequencies and peripheral preference for lower spatial frequencies. However, visual information processing in V2v through V3v appears to occur at a progressively coarser scale, i.e., spatial frequency tuning becomes coarser than in V1. For example, in V3v the data indicate a decline in response across eccentricity even at 0.55 cpd, the spatial frequency used by Mullen et al. [48]. In V1, there is an increase in response across eccentricity for the same spatial frequency. Overall, it appears that eccentricity-related |L-M| sensitivity loss does not occur in V1 through V3v.

B. Eccentricity and magnification factor

For the assessment of local cortical magnification factors we used an indirect approach where stimulus size and location were kept constant and only spatial-frequency content varied. Estimates of the cortical magnification factor were then obtained by comparing the spatial-frequency tuning curves at the different eccentricities. This worked well for V1 but not for the later areas, largely because in those areas spatial tuning was coarser, and the range of spatial frequencies used was not wide enough to always capture the tuning function's peak. Within V1 the range sufficed, however; the resulting inverse-linear functions and their E2 values for the |L-M| and Lum channels corresponded roughly to those previously obtained with achromatic stimuli, both in fMRI and psychophysical studies (see Strasburger et al. [1], Section 3.2, for review). Note that a numerical comparison of E2 values obtained across different approaches is limited by the fact that, particularly in those from cortical location maps (e.g. Larsson & Heeger [69]), E2 and M0 (i.e. foveal M) estimates are strongly negatively correlated, such that these values are meaningful only as a pair.

Responses in V1 showed a similar spatial tuning for achromatic (Lum) and |L-M| responses as a function of eccentricity (Fig. 4). This is consistent with the same rules governing eccentricity scaling in V1 for both |L-M| and achromatic signals. The original M-scaling concept was directly based on density of retinal elements and their representation in V1 [16]. Both PC- and MC-pathways derive receptor input from the M- and L-cones, with little or no S-cone input [80]. The ratio of cone to ganglion cell density remains similar from fovea to mid-periphery, as does the proportion of parasol (MC) to midget (PC) ganglion cells [25, 81]. However, the scaling function for the S-cone response in V1 (Fig. 5F) is different from the others. It appears shallower, which implies that spatial tuning scales less rapidly than the others toward the periphery.

Anatomical and physiological studies have provided evidence that blue-yellow cone-opponency passes through a separate pathway originating in the small bistratified ganglion cell type of the retina as well as other cell types [23, 82, 83]. This pathway remains distinct through the koniocellular layers of the LGN and to the blobs of V1. S-cones are absent in the center of the tritanopic fovea, then increase rapidly relative to M- and L-cones up to ca. 6–7 deg eccentricity; beyond this point their proportion stabilizes and remains relatively constant (at about 7%; [41]).

We attempted to analyze the change in scaling, based on estimates of cone density of Curcio and collaborators [41, 84]. The analysis assumed that the density of S-cone ganglion cells is proportional to S-cone density, and that convergence of S-cone LGN cells onto cortical neurons is determined by the density of input from S-cone cells in the LGN rather than cortical magnification per se. Calculations based on S-cone density predict a flattening of the E2 relation for the S-cone compared to that for the M,L cones. There were considerable uncertainties in this analysis, but it is consistent with the idea that S cone percentage will affect the scaling of optimal spatial frequency of S-cone chromatic mechanisms, and that this might be different from to achromatic and |L-M| mechanisms, at least partly accounting for our data.

C. Psychophysical considerations

Color naming experiments showed that color naming was fairly normal in the peripheral visual field [2-4], countering earlier suggestions that color vision was poor or nonexistent in the periphery. Nevertheless, there is considerable evidence that |M-L| contrast sensitivity declines with eccentricity more rapidly than does achromatic sensitivity [6, 7, 33], and it was proposed that this was associated with random connectivity of midget bipolars to midget ganglion cells with increasing convergence at higher eccentricities [9]. To bolster this hypothesis, it is desirable to show that psychophysical sensitivity of the |L-M| chromatic channel declines more rapidly than sensitivity of a channel based on S-cone sensitivity. Some studies show that this is the case [5, 10, 11], although none of them specifically consider the possibility of different spatial scaling of the S-cone mechanism. Nevertheless, at least in one study [10] the range of spatial frequencies investigated should have compensated for difficulties from this source, and eccentricities extended well beyond 10 deg. Some psychophysical studies have specifically targeted the possibility of different scalings with eccentricity based on cone densities. Volbrecht et al. [43] found Riccò's area for S-cone stimuli to change differently with eccentricity compared with achromatic or |L-M| mechanisms, and tried to explain this with the differential distributions of cones. Vakrou et al. [42] found that psychophysical contrast sensitivity curves based on S-cone activity scaled less rapidly with eccentricity than those for the other two modalities, qualitatively resembling our data.

As in many cases when physiology is related to neural models for psychophysical data [85], the neurobiological foundations for behavioral results may be more complex than anticipated. We show here evidence for a different physiological scaling with eccentricity for the S-cone mechanism compared to the other two modalities, a factor that has largely been neglected. Finally, we would stress that one-to-one midget connectivity is well maintained up to 10 deg and beyond [78], an eccentricity at which a decrease in |L-M| psychophysical sensitivity is already apparent [10]. This decrease must presumably have a central locus; it remains to be seen whether, with appropriately scaled

stimuli, S-cone psychophysical sensitivity shows a similar change. In any event, it seems likely that changes in chromatic (and achromatic) psychophysical sensitivity with eccentricity derive from both retinal and cortical substrates.

Funding. National Institutes of Health NEI R01-13112 (BBL)

Acknowledgements. We thank Dietmar Merboldt, Dirk Voit, Lutz Präkelt, Kurt Böhm, and Henry Lütcke for technical assistance.

REFERENCES

1. H. Strasburger, I. Rentschler, and M. Juttner, "Peripheral vision and pattern recognition: a review," J Vision **11**, 13 (2011).
2. I. Abramov and J. Gordon, "Color vision in the peripheral retina II, Hue and saturation," JOSA **67**, 202-206 (1977).
3. C. Noorlander, J. J. Koenderink, R. J. den Ouden, and B. W. Edens, "Sensitivity to spatiotemporal colour contrast in the peripheral visual field," Vision Res. **23**, 1-11 (1983).
4. I. Abramov, J. Gordon, and H. Chan, "Color appearance in the peripheral retina: effects of stimulus size," JOSA A. **8**, 404-414 (1991).
5. T. Hansen, L. Pracejus, and K. R. Gegenfurtner, "Color perception in the intermediate periphery of the visual field," J Vision **9**, 26 21-12 (2009).
6. S. J. Anderson, K. T. Mullen, and R. F. Hess, "Human peripheral spatial resolution for achromatic and chromatic stimuli: limits imposed by optical and retinal factors," J Physiol **442**, 47-64 (1991).
7. K. T. Mullen, "Colour vision as a post-receptoral specialization of the central visual field," Vision Res **31**, 119-130 (1991).
8. C. F. Stromeyer, 3rd, J. Lee, and R. T. Eskew, Jr., "Peripheral chromatic sensitivity for flashes: a post-receptoral red-green asymmetry," Vision Res **32**, 1865-1873 (1992).
9. K. T. Mullen and F. A. Kingdom, "Losses in peripheral colour sensitivity predicted from "hit or miss" post-receptoral cone connections," Vision Res **36**, 1995-2000 (1996).
10. K. T. Mullen and F. A. Kingdom, "Differential distributions of red-green and blue-yellow cone opponency across the visual field," Vis Neurosci **19**, 109-118 (2002).
11. K. T. Mullen, M. Sakurai, and W. Chu, "Does L/M cone opponency disappear in human periphery?," Perception **34**, 951-959 (2005).
12. J. J. Koenderink, M. A. Bouman, A. E. Bueno de Mesquita, and S. Slappendel, "Perimetry of contrast detection thresholds of moving spatial sine wave patterns. III. The target extent as a sensitivity controlling parameter," JOSA. **68**, 854-860 (1978).
13. J. J. Koenderink, M. A. Bouman, A. E. Bueno de Mesquita, and S. Slappendel, "Perimetry of contrast detection thresholds of moving spatial sine patterns. II. The far peripheral visual field (eccentricity 0 degrees-50 degrees)," JOSA **68**, 850-854 (1978).
14. J. J. Koenderink, M. A. Bouman, A. E. Bueno de Mesquita, and S. Slappendel, "Perimetry of contrast detection thresholds of moving spatial sine wave patterns. I. The near peripheral visual field (eccentricity 0 degrees-8 degrees)," JOSA **68**, 845-849 (1978).
15. J. Rovamo and V. Virsu, "An estimation and application of the human cortical magnification factor," Exp Brain Res **37**, 495-510 (1979).
16. V. Virsu and J. Rovamo, "Visual resolution, contrast sensitivity, and the cortical magnification factor.," Exp Brain Res **37**, 475-494 (1979).
17. V. Virsu, R. Näsänen, and K. Osmoviita, "Cortical magnification and peripheral vision," JOSA A. **4**, 1568-1578 (1987).
18. P. M. Daniel and D. Whitteridge, "The representation of the visual field on the cerebral cortex in monkeys," J Physiol **159**, 203-221 (1961).
19. A. Cowey and E. T. Rolls, "Human cortical magnification factor and its relation to visual acuity," Exp Brain Res **21**, 447-454 (1974).
20. D. M. Levi, S. A. Klein, and A. P. Aitsebaomo, "Vernier acuity, crowding and cortical magnification," Vision Res **25**, 963-977 (1985).
21. R. L. DeValois, C. Morgan, M. C. Polson, W. R. Mead, and E. M. Hull, "Psychophysical studies of monkey vision-I. Macaque luminosity and color vision tests," Vision Res **14**, 53-67 (1974).
22. R. L. DeValois, H. Morgan, and D. M. Snodderly, "Psychophysical studies of monkey vision - III. Spatial luminance contrast sensitivity tests of macaque and human observers," Vision Res **14**, 75-81 (1974).
23. B. B. Lee, "Visual pathways and psychophysical channels in the primate," J Physiol **589**, 41-47 (2011).
24. T. Wiesel and D. H. Hubel, "Spatial and chromatic interactions in the lateral geniculate body of the rhesus monkey," J Neurophysiol **29**, 1115-1156 (1966).
25. H. Wässle and B. B. Boycott, "Functional architecture of the mammalian retina," Physiol Rev **71**, 447-480 (1991).
26. R. C. Reid and R. M. Shapley, "Spatial structure of cone inputs to receptive fields in primate lateral geniculate nucleus," Nature **356**, 716-718 (1992).
27. D. J. Calkins, S. J. Schein, Y. Tsukamoto, and P. Sterling, "M and L cones in macaque fovea connect to midget ganglion cells by different numbers of excitatory synapses," Nature **371**, 70-72 (1994).
28. B. B. Lee, J. Kremers, and T. Yeh, "Receptive fields of primate ganglion cells studied with a novel technique," Vis Neurosci **15**, 161-175 (1998).
29. R. C. Reid and R. M. Shapley, "Space and time maps of cone photoreceptor signals in macaque lateral geniculate nucleus," J Neurosci **22**, 6158-6175 (2002).
30. B. B. Lee, R. M. Shapley, M. J. Hawken, and H. Sun, "The spatial distributions of cone inputs to cells of the parvocellular pathway investigated with cone-isolating gratings," JOSA A (2012).
31. B. B. Boycott and J. E. Dowling, "Organization of the primate retina: Light microscopy," Phil Trans Roy Soc Lond B **255**, 109-184 (1969).
32. H. Wässle, U. Grünert, P. R. Martin, and B. B. Boycott, "Color coding in the primate retina: predictions and constrants from anatomy," in *Structural and functional organization of the neocortex. A symposium in the memory of Otto D. Creutzfeldt*, B. Albowitz, K. Albus, U. Kuhnt, H. C. Nothdurft, and P. Wahle, eds. (Springer, Berlin, Heidelberg, New York, 1994), pp. 94-104.

33. J. R. Newton and R. T. Eskew, Jr., "Chromatic detection and discrimination in the periphery: a postreceptoral loss of color sensitivity," Vis Neurosci **20**, 511-521 (2003).
34. P. R. Martin, B. B. Lee, A. J. White, S. G. Solomon, and L. Rüttiger, "Chromatic sensitivity of ganglion cells in peripheral primate retina," Nature **410**, 933-936 (2001).
35. S. G. Solomon, B. B. Lee, A. J. White, L. Ruttiger, and P. R. Martin, "Chromatic organization of ganglion cell receptive fields in the peripheral retina," J Neurosci **25**, 4527-4539 (2005).
36. J. D. Crook, M. B. Manookin, O. S. Packer, and D. M. Dacey, "Horizontal cell feedback without cone type-selective inhibition mediates "red-green" color opponency in midget ganglion cells of the primate retina," J Neurosci **31**, 1762-1772 (2011).
37. G. D. Field, J. L. Gauthier, A. Sher, M. Greschner, T. A. Machado, L. H. Jepson, J. Shlens, D. E. Gunning, K. Mathieson, W. Dabrowski, L. Paninski, A. M. Litke, and E. J. Chichilnisky, "Functional connectivity in the retina at the resolution of photoreceptors," Nature **467**, 673-677 (2010).
38. A. M. Derrington, J. Krauskopf, and P. Lennie, "Chromatic mechanisms in lateral geniculate nucleus of macaque," J. Physiol. (Lond). **357**, 241-265 (1984).
39. A. M. Derrington and P. Lennie, "Spatial and temporal contrast sensitivities of neurones in lateral geniculate nucleus of macaque," J Physiol **357**, 219-240 (1984).
40. W. H. Swanson, H. Sun, B. B. Lee, and D. Cao, "Responses of Retinal Ganglion Cells to Perimetric Stimuli," Inv. Ophth Vis Sci **51**(2010).
41. C. A. Curcio, A. A. Kimberly, K. R. Sloan, C. L. Lerea, J. B. Hurley, I. B. Klock, and A. H. Milam, "Distribution and morphology of human cone photoreceptors stained with anti-blue opsin," J Comp Neurol **312**, 610-624 (1991).
42. C. Vakrou, D. Whitaker, P. V. McGraw, and D. McKeefry, "Functional evidence for cone-specific connectivity in the human retina," J Physiol **566**, 93-102 (2005).
43. V. J. Volbrecht, E. E. Shrago, B. E. Schefrin, and J. S. Werner, "Spatial summation in human cone mechanisms from 0 degrees to 20 degrees in the superior retina," JOSA A. **17**, 641-650 (2000).
44. A. Kleinschmidt, B. B. Lee, M. Requardt, and J. Frahm, "Functional mapping of color processing by magnetic resonance imaging of responses to selective P- and M-pathway stimulation," Exp Brain Res **110**, 279-288 (1996).
45. J. Liu and B. A. Wandell, "Specializations for chromatic and temporal signals in human visual cortex," J Neurosci **25**, 3459-3468 (2005).
46. S. Engel, X. Zhang, and B. Wandell, "Colour tuning in human visual cortex measured with functional magnetic resonance imaging," Nature **388**, 68-71 (1997).
47. K. D. Singh, A. T. Smith, and M. W. Greenlee, "Spatiotemporal frequency and direction sensitivities of human visual areas measured using fMRI," Neuroimage **12**, 550-564 (2000).
48. K. T. Mullen, S. O. Dumoulin, K. L. McMahon, G. I. de Zubicaray, and R. F. Hess, "Selectivity of human retinotopic visual cortex to S-cone-opponent, L/M-cone-opponent and achromatic stimulation," Eur J Neurosci **25**, 491-502 (2007).
49. A. Wade, M. Augath, N. Logothetis, and B. Wandell, "fMRI measurements of color in macaque and human," J Vision **8**, 1-19 (2008).
50. K. T. Mullen, B. Thompson, and R. F. Hess, "Responses of the human visual cortex and LGN to achromatic and chromatic temporal modulations: an fMRI study," J Vision **10**, 13 (2010).
51. D. V. D'Souza, T. Auer, H. Strasburger, J. Frahm, and B. B. Lee, "An fMRI study of chromatic processing in humans: Temporal characteristics of cortical visual areas " J Vision **11**, 1-17 (2011).
52. L. Henriksson, L. Nurminen, A. Hyvarinen, and S. Vanni, "Spatial frequency tuning in human retinotopic visual areas," J Vision **8**, 1-13 (2008).
53. S. Vanni, L. Henriksson, M. Viikari, and A. C. James, "Retinotopic distribution of chromatic responses in human primary visual cortex," Eur J Neurosci **24**, 1821-1831 (2006).
54. H. Strasburger, T. Wustenberg, and L. Jancke, "Calibrated LCD/TFT stimulus presentation for visual psychophysics in fMRI," J Neurosci Methods **121**, 103-110 (2002).
55. V. C. Smith and J. Pokorny, "Spectral sensitivity of the foveal cone photopigments between 400 and 500 nm," Vision Res **15**, 161-171 (1975).
56. E. A. DeYoe, G. J. Carman, P. Bandettini, S. Glickman, J. Wieser, R. Cox, D. Miller, and J. Neitz, "Mapping striate and extrastriate visual areas in human cerebral cortex," Proc Natl Acad Sci **93**, 2382-2386 (1996).
57. S. A. Engel, D. E. Rumelhart, B. A. Wandell, A. T. Lee, G. H. Glover, E. J. Chichilnisky, and M. N. Shadlen, "fMRI of human visual cortex," Nature **369**, 525 (1994).
58. D. E. Linden, U. Kallenbach, A. Heinecke, W. Singer, and R. Goebel, "The myth of upright vision. A psychophysical and functional imaging study of adaptation to inverting spectacles," Perception **28**, 469-481 (1999).
59. H. Lu, G. Basso, J. T. Serences, S. Yantis, X. Golay, and P. C. van Zijl, "Retinotopic mapping in the human visual cortex using vascular space occupancy-dependent functional magnetic resonance imaging," Neuroreport **16**, 1635-1640 (2005).
60. E. A. DeYoe, P. Bandettini, J. Neitz, D. Miller, and P. Winans, "Functional magnetic resonance imaging (FMRI) of the human brain," J Neurosci Methods **54**, 171-187 (1994).
61. M. I. Sereno, A. M. Dale, J. B. Reppas, K. K. Kwong, J. W. Belliveau, T. J. Brady, B. R. Rosen, and R. B. Tootell, "Borders of multiple visual areas in humans revealed by functional magnetic resonance imaging," Science **268**, 889-893 (1995).
62. G. M. Boynton, S. A. Engel, G. H. Glover, and D. J. Heeger, "Linear systems analysis of functional magnetic resonance imaging in human V1," J Neurosci **16**, 4207-4221 (1996).
63. T. P. Hicks, B. B. Lee, and T. R. Vidyasagar, "The responses of cells in macaque lateral geniculate nucleus to sinusoiodal gratings," J Physiol **337**, 183-200 (1983).
64. B. B. Lee, H. Sun, and A. Valberg, "Segregation of chromatic and luminance signals using a novel grating stimulus," J Physiol **589**, 59-73 (2011).
65. A. B. Watson, "Estimation of local spatial scale," JOSA A. **4**, 1579-1582 (1987).
66. N. Drasdo, "Neural substrates and threshold gradients of peripheral vision," in *Limits of Vision*, J. J. Kulikowski, V. Walsh, and I. J. Murray, eds. (MacMillan Press, London, 1991), pp. 250-264.
67. F. W. Weymouth, "Visual sensory units and the minimal angle of resolution," Am J Ophthal **46**, 102-113 (1958).

68. R. F. Dougherty, V. M. Koch, A. A. Brewer, B. Fischer, J. Modersitzki, and B. A. Wandell, "Visual field representations and locations of visual areas V1/2/3 in human visual cortex," J Vision **3**, 586-598 (2003).
69. J. Larsson and D. J. Heeger, "Two retinotopic visual areas in human lateral occipital cortex," J Neurosci **26**, 13128-13142 (2006).
70. M. M. Schira, A. R. Wade, and C. W. Tyler, "Two-dimensional mapping of the central and parafoveal visual field to human visual cortex," J Neurophysiol **97**, 4284-4295 (2007).
71. M. M. Schira, C. W. Tyler, M. Breakspear, and B. Spehar, "The foveal confluence in human visual cortex," J Neurosci **29**, 9050-9058 (2009).
72. J. B. Levitt, D. C. Kiper, and J. A. Movshon, "Receptive fields and functional architecture of macaque V2," J Neurophysiol **71**, 2517-2542 (1994).
73. A. T. Smith, K. D. Singh, A. L. Williams, and M. W. Greenlee, "Estimating receptive field size from fMRI data in human striate and extrastriate visual cortex," Cereb Cortex **11**, 1182-1190 (2001).
74. K. A. Hansen, K. N. Kay, and J. L. Gallant, "Topographic organization in and near human visual area V4," J Neurosci **27**, 11896-11911 (2007).
75. A. R. Wade, A. A. Brewer, J. W. Rieger, and B. A. Wandell, "Functional measurements of human ventral occipital cortex: retinotopy and colour," Phil Trans Roy Soc Lond B. Biol. Sci. **357**, 963-973 (2002).
76. B. A. Wandell and J. Winawer, "Imaging retinotopic maps in the human brain," Vision Res **51**, 718-737 (2011).
77. C. W. Tyler, L. T. Likova, C. C. Chen, L. L. Kontsevich, M. M. Schira, and A. W. Wade, "Extended concepts of occipital retinotopy," Current Medical Imaging Reviews **1**, 319-329 (2005).
78. B. B. Lee, P. R. Martin, and U. Grünert, "Retinal connectivity and primate vision," Prog Ret Res **29**, 622-639 (2010).
79. K. T. Mullen, S. O. Dumoulin, and R. F. Hess, "Color responses of the human lateral geniculate nucleus: selective amplification of S-cone signals between the lateral geniculate nucleno and primary visual cortex measured with high-field fMRI," Eur J Neurosci **28**, 1911-1923 (2008).
80. H. Sun, H. Smithson, Q. Zaidi, and B. B. Lee, "Specificity of cone inputs to macaque ganglion cells," J Neurophysiol **95**, 837-849 (2006).
81. U. Grünert, U. Greferath, B. B. Boycott, and H. Wässle, "Parasol (Pa) ganglion cells of the primate fovea: Immunocytochemical staining with antibodies against $GABA_A$ - receptors," Vision Res **33**, 1-14 (1993).
82. D. M. Dacey and B. B. Lee, "The blue-ON opponent pathway in primate retina originates from a distinct bistratified ganglion cell type," Nature **367**, 731-735 (1994).
83. P. R. Martin and B. B. Lee, "Distribution and specificity of S-cone ("blue cone") signals in subcortical visual pathways," Vis Neurosci **31**, 177-187 (2014).
84. C. A. Curcio, K. R. Sloan, R. E. Kalina, and A. E. Hendrickson, "Human photoreceptor topography," J Comp Neurol **292**, 497-523 (1990).
85. B. B. Lee, "Neural models and physiological reality," Vis Neurosci **251**, 231-241 (2008).